accepted for IEEE/RSJ IROS 2013

Slip Interface Classification through Tactile Signal Coherence

Barrett Heyneman and Mark R. Cutkosky

***Abstract*— The manipulation of objects in a hand or gripper is typically accompanied by events such as slippage, between the fingers and a grasped object or between the object and external surfaces. Humans can identify such events using a combination of superficial and deep mechanoreceptors. In robotic hands, with more limited tactile sensing, such events can be hard to distinguish. This paper presents a signal processing method that can help to distinguish finger/object and object/world events based on multidimensional coherence, which measures whether a group of signals are sampling a single input or a group of incoherent inputs. A simple linear model of the fingertip/object interaction demonstrates how signal coherence can be used for slip classification. The method is evaluated through controlled experiments that produce similar results for two very different tactile sensing suites.**

***Index Terms*— tactile sensing, slip, manipulation**

I. Introduction

When manipulating a grasped object, events such as making or breaking contact, and slippage, can occur between the fingers and the object or between the object and external surfaces. These events are ubiquitous in human manipulation and provide us with important information about how a task is proceeding. In many tasks, such as when assembling or disassembling parts, or inserting a key into a lock, one event signals success while another indicates failure. In order to implement manipulation strategies that react to these events quickly and appropriately, robots must have a way to distinguish between them.

The majority of research in robotic tactile sensing has focused on finger/object interactions. Recent reviews include [1], [2], [3]. Numerous methods have been proposed for detecting slips, and the small vibrations that accompany incipient slippage between a finger and an object, in order to react to or control slip during manipulation [4], [5], [6], [7]. Other related work has focused on using information obtained by sliding a finger or instrument over a surface to recognize different textures as part of exploration, [8], [9], [10], [11], [12].

Humans easily distinguish between finger/object and object/world slips because they have different effects on mechanoreceptors in the skin. In particular, FA-I (fast-acting, type one) mechanoreceptors are strongly responsive to localized slips produced by interactions between the dermal papillae and the surface of an object, while deeper FA-II mechanoreceptors are particularly receptive to vibrations propagating through the tissues of the hand, such as those produced by a tool interacting with the environment [13], [14].

The authors are with the Dept. of Mechanical Engineering, Stanford University, Stanford, CA, USA. heyneman, cutkosky @stanford.edu

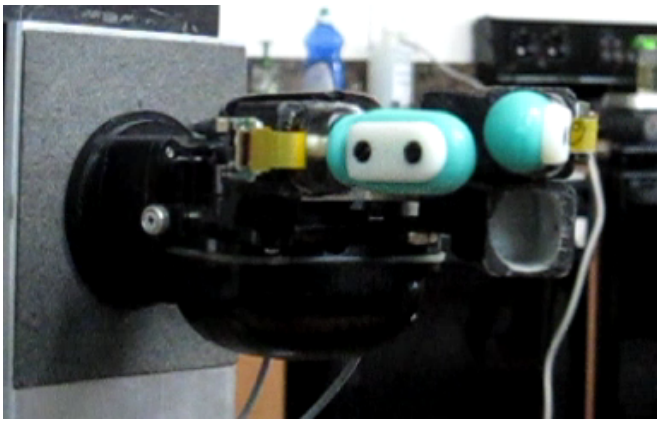

Fig. 1: Two BioTac fingertip sensors are mounted on opposing fingers of a Motion Control Hand. The fingers are passively loaded to provide grip force on objects while various slip conditions are produced between the BioTacs and the held object or between the object and external stimuli.

Our prior work on slip classification [15] used a measure of relative power between individual tactile sensors in an array (localized events) and the entire array as an ensemble (large receptive field). This paper presents a new signal processing method for tactile array sensors aimed at distinguishing hand/object slippage from object/world slippage for a variety of textures, conditions, and sensor technologies. It is motivated by additional observations from biology concerning relative timing and phasing of neural activity:

- the coincidence of initial neural spikes from mechanoreceptors in the human hand encodes information about object properties such as friction or texture [16];
- neural activity during the deformation in halteres of flying insects is phase-locked to wing flapping [17];
- coherence of pacinian corpuscle activity encodes vibratory information in a cat's footpad [18].

The new approach is based on a multidimensional version of the classical definition of signal coherence which indicates the degree to which individual sensors are sampling a common underlying signal (e.g. the vibration of a held object). The applicability of the method to different sensing technologies is investigated in experiments using two very different sensors: a custom piezo-film-based tactile array and the BioTac™ sensor (SynTouch LLC) [19].

II. Tactile Signal Coherence

To distinguish between hand/object and object/world slip events, we begin by considering how the vibration source differs in the two cases, and how that difference affects the tactile array. During hand/object slippage, vibrations are generated by complex stick-slip phenomena. These vibrations originate first at the edge of the contact patch between the hand and object during "incipient slip" [4] and then across the entire contact patch during gross slip. Because the relative timing of the individual stick slip events depends on local contact geometry, contact pressure, surface roughness, etc., the sensor array measures *multiple independent vibration sources*. In contrast, object/world slippage causes vibration of the held object. This *single source* then excites the sensor array.

In this section we briefly review the properties of *complex coherence* and *mean square coherence* (a full treatment can be found in e.g. [20]) and show how those properties can be used in slip classification. A generalization of mean square coherence to n signals is derived by determining how much of the group signal content can be explained by a single underlying signal. This derivation is consistent with the classical definition in the $n = 2$ case and can be used with practical arrays of tactile sensors ($n > 2$).

A. Power Spectra and Coherence

A multivariate signal $\boldsymbol{x}$ has a *power spectral density matrix* $\mathcal{P}_x(\omega)$ defined for each frequency ω, with the *power spectrum* of individual signals x_i on the diagonal and the *cross spectral density* between individual signals on the off-diagonals. The *complex coherence* between two signals $\boldsymbol{x}_i$ and $\boldsymbol{x}_j$ is defined as the cross spectral density normalized with respect to each signal's power spectrum; therefore the entries in the *complex coherence matrix*, $\mathcal{C}_x(\omega)$ are given by

$$\mathcal{C}_{ij}(\omega) = \frac{\mathcal{P}_{ij}(\omega)}{\sqrt{\mathcal{P}_{ii}(\omega)}\sqrt{\mathcal{P}_{jj}(\omega)}} \tag{1}$$

From this definition, and because $\mathcal{P}_x$ is a Hermitian matrix, $\mathcal{C}_x$ has the following properties:

- the diagonals are 1, $\mathcal{C}_{ii} = 1$
- off diagonal magnitude is bounded, $|\mathcal{C}_{ij}(\omega)| \leq 1$
- the eigenvalues are positive reals, $\lambda(\mathcal{C}_x) > 0, \in \mathbb{R}$.

In general use, "coherence" typically refers to the *mean square coherence* between the signals, $\mathcal{C}_{ij}^2$, defined as $|\mathcal{C}_{ij}|^2$. This quantity lies in the range $[0, 1]$ and can be interpreted as:

- the correlation between signals at each frequency,
- the constancy of relative phasing between signals at each frequency,
- the degree to which one signal is a linearly filtered version of the other, at each frequency.

In this analysis we make use of the following result. When a multivariate signal $\boldsymbol{y}$ is a linearly filtered version of another multivariate signal $\boldsymbol{x}$, with $\boldsymbol{y}(t) = (\boldsymbol{H} * \boldsymbol{x})(t)$, then the power spectral density matrix of $\boldsymbol{y}$ is given by

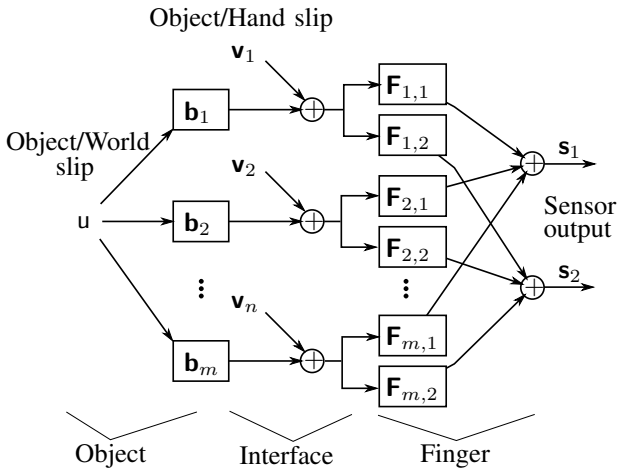

Fig. 2: A full system model including motion/vibration of a held object, the interface between that object and a finger, and the mechanics of the finger.

$$\mathcal{P}_y(\omega) \quad = \quad \mathbf{H}(\omega)\mathcal{P}_x(\omega)\mathbf{H}^H(\omega) \tag{2}$$

B. Two Sensor Model

We begin by constructing a simple linear model of the world, object, hand, and sensor array system. A rigid object is in contact with both an external, world object and a textured tactile sensor with two embedded sensors. It is convenient to consider the sensors as measuring surface strain because many existing tactile sensors follow this model and strain is additive. Formally, we make the following assumptions:

1) The held object is rigid.
2) The surface of the skin is textured and makes contact with the object in a finite number of locations, m.
3) The variation of interface conditions (texture, contact pressure, etc) between locations is negligible.
4) The transduction path from surface strain at contact location i to sensor j can be modeled as a linear, time invariant system with transfer function $\mathbf{F}_{ij}$.

The expanded block diagram for this system is shown in Fig. 2 with individual single-input-single-output transfer functions shown. Vibrations caused by slip between the object and the world generate a single signal, u, which propagates to the m contact locations through the body transfer functions, $\mathbf{b}_i$. The strain at those locations is then added to any strain due to slippage at the object/hand interface, $\mathbf{v}_i$. Finally, the finger mechanics are modeled as the transfer functions $\mathbf{F}_{ij}$, which determine the sensor outputs.

This model can be greatly simplified using multi-input-multi-output transfer functions, yielding

$$\mathbf{s} = \mathbf{F}^T(\mathbf{b}\mathsf{u} + \mathbf{v}) \tag{3}$$

where $\mathbf{F} \in \mathbb{C}^{m\times 2}$ describes the finger dynamics, $\mathbf{b} \in \mathbb{C}^m$ describes the coupling between object and finger, $\mathbf{s} \in \mathbb{C}^2$ is the array output, and $\mathsf{u} \in \mathbb{C}$ and $\mathbf{v} \in \mathbb{C}^m$ are the input

vibrations due to the object/world slippage and object/hand slippage, respectively.

Next we investigate how the two slippage cases affect the coherence between the two sensor signals.

1) Object/World Slippage: In the case where there is only object/world slippage the $\mathbf{v}$ term drops out of Eqn. (3) and we are left with $\mathbf{s} = \mathbf{F}^T\mathbf{b}\mathsf{u}$. Using Eqn. (2) we can compute the spectral density matrix for the sensor output as

$$\mathcal{P}_s = \left(\mathbf{F}^T\mathbf{b}\right)\mathcal{P}_u\left(\mathbf{F}^T\mathbf{b}\right)^H \quad (4)$$

$$= \mathcal{P}_u\left(\mathbf{F}^T\mathbf{b}\right)\left(\mathbf{F}^T\mathbf{b}\right)^H \quad (5)$$

where we have used the fact that $\mathcal{P}_u \in \mathbb{R}$.

Because $\mathbf{F}^T\mathbf{b} \in \mathbb{C}^2$ we have $\operatorname{rank}(\mathcal{P}_s) = 1$; therefore when $\mathcal{P}_s$ is normalized per Eqn. (1) it yields

$$\mathcal{C}_s = \begin{bmatrix} 1 & 1 \\ 1 & 1 \end{bmatrix} \quad (6)$$

$$\mathcal{C}_{s_1 s_2} = 1 \quad (7)$$

This indicates that the two sensor signals are maximally coherent when they are both filtered versions of a single signal. The result is entirely in keeping with the interpretations of coherence outlined above.

2) Object/Hand Slip: When there is only object/hand slippage the u term drops out of Eqn. (3), leaving $\mathbf{s} = \mathbf{F}\mathbf{v}$. Some additional assumptions about the signals and transfer functions are required:

- *Zero Cross-Talk*: The column vectors of $\mathbf{F}$ representing the transfer functions from contacts to each sensor are orthogonal; $\mathbf{F}_1^H\mathbf{F}_2 = 0$.
- *Identical and Independent*: Each vibration signal v_i is due to independent stick-slip events subject to identical contact conditions. Therefore each v_i has the same power spectrum but has zero coherence with any other signal v_j; $\mathcal{P}_v = \mathsf{p_v}\mathbf{I}$.

Using these assumptions and Eqn. (2) leads to the following expression for the sensor spectral density matrix.

$$\mathcal{P}_s = \mathbf{F}^H\mathcal{P}_v\mathbf{F} \quad (8)$$

$$= \mathsf{p_v}\mathbf{F}^H\mathbf{F} \quad (9)$$

The off-diagonals of $\mathbf{F}^H\mathbf{F}$ are zero due to the zero cross-talk assumption, such that normalizing the matrix results in

$$\mathcal{C}_s = \begin{bmatrix} 1 & 0 \\ 0 & 1 \end{bmatrix} \quad (10)$$

$$\mathcal{C}_{s_1 s_2} = 0 \quad (11)$$

This indicates that when the sensors measure multiple incoherent input signals with zero crosstalk between them, the sensor outputs are minimally coherent.

The assumptions made for this model will be violated in practice. During real manipulations slip may occur at both interfaces. Soft robot fingers may undergo large strains which violate simple linear elastic models of the transduction paths from contact strain to sensor readings. The contact conditions will not be identical at every location, nor will the vibrations generated be completely incoherent. Finally, while zero sensor crosstalk is always desired, it is very rarely achieved in the design of tactile sensing arrays due to the physical coupling induced by the finger medium.

However, this analysis does demonstrate that during object/world slip, when there is primarily one source of vibration, the coherence between sensor signals should be large relative to that during object/hand slip, when there are multiple sources of vibration.

C. Generalized Coherence

The preceding two-sensor example leads to a different interpretation of mean square coherence which generalizes to n sensors: *the maximum fraction of normalized observed signal power explained by a linear systems model with a single input.*

In this section we derive this result in the general case and show that it can be computed with a simple eigenvalue analysis of the complex coherence matrix. We then verify that it is equivalent to the classical definition in the $n = 2$ case and verify its results for some limiting cases.

The n signals, $s_i(t)$ are estimated by filtering a common input signal, x:

$$\hat{s}_i(t) = (h_i * x)(t) \quad (12)$$

with $h_i(t)$ being the impulse response of the ith filter. The error signal $e_i(t)$ is given by

$$e_i(t) = s_i(t) - \hat{s}_i(t) \quad (13)$$

$$= s_i(t) - (h_i * u)(t) \quad (14)$$

We seek to maximize the following objective function at all frequencies, ω

$$\max_{u,h} J(\omega) = \left(1 - \frac{1}{n-1}\sum_{i=1}^{n}\frac{\mathcal{P}_{e_i}(\omega)}{\mathcal{P}_{s_i}(\omega)}\right)^2 \quad (15)$$

The terms within the summation are normalized error powers; they are averaged by a factor of $n-1$ instead of n because there always exists a signal and filter pair which makes one error term identically zero; e.g. $x(t) = s_i(t)$, $h_i(t) = \delta(t)$ results in $e_i(t) = 0$. This normalized and averaged error is then subtracted from 1, leaving a normalized measure of signal power explained by the linear model.

Maximizing Eqn. (15) is equivalent to minimizing the sum of the normalized error, J_{eq}. Because there is no restriction on x or h, this optimization can be performed independently at each frequency; subsequent ω arguments have been omitted for clarity.

$$J_{eq} = \sum_{i=1}^{n}\frac{\mathcal{P}_{e_i}}{\mathcal{P}_{s_i}} \quad (16)$$

$$= \sum_{i=1}^{n}\frac{\mathcal{P}_{s_i} - \mathsf{h}_i^H\mathcal{P}_x\mathsf{h}_i}{\mathcal{P}_{s_i}} \quad (17)$$

Without loss of generality we can assume that x is a white-noise input with unit power at all frequencies. If we let $\mathbf{D}_s = \mathrm{diag}(\mathcal{P}_s)$ be the matrix with each signal power on the diagonals, the objective can be expressed as

$$J_{eq} = \mathrm{Tr}\left(\mathbf{D}^{-1/2}\left(\mathcal{P}_s - \mathbf{h}^H\mathbf{h}\right)\mathbf{D}^{-1/2}\right) \quad (18)$$

$$= \sum_{i=1}^{n}\lambda\left(\mathcal{C}_s - \mathbf{D}^{-1/2}\mathbf{h}^H\mathbf{h}\mathbf{D}^{-1/2}\right) \quad (19)$$

where we have used the fact that the trace of a matrix is the sum of its eigenvalues. J_{eq} is minimized when $\mathbf{h}\mathbf{D}^{-1/2} = \lambda^{1/2}v_1$, where λ_1 is the largest eigenvalue of the complex coherence matrix $\mathcal{C}_s$ and v_1 is the corresponding eigenvector. This yields

$$\min_h J_{eq} = \sum_{i=2}^{n}\lambda\left(\mathcal{C}_s\right) = n - \lambda_1 \quad (20)$$

Substituting Eqn. (20) into Eqn. (15) and simplifying we find a new, generalized definition for mean square coherence:

$$\mathcal{C}_s^2 \equiv \max_h J = \left(1 - \frac{1}{n-1}\left(\min_h J_{eq}\right)\right)^2 = \left(\frac{\lambda_1 - 1}{n-1}\right)^2 \quad (21)$$

1) Verification for $n = 2$ Case: The general form of the complex coherence matrix for $n = 2$ is

$$\mathcal{C}_s = \begin{bmatrix} 1 & c \\ c^* & 1 \end{bmatrix} \quad (22)$$

where c and c^* are the complex coherence values between the two signals and $\mathcal{C}_{s_1 s_2}^2 = |c|^2$ as per Eqn. (1).

The eigenvalues of $\mathcal{C}_s$ are $\lambda_1\left(\mathcal{C}_s\right) = 1 + |c|$ and $\lambda_2 = 1 - |c|$. Substituting λ_1 into Eqn. (21) yields

$$\mathcal{C}_s^2 = \left(\frac{1 + |c| - 1}{2 - 1}\right)^2 = |c|^2 \quad (23)$$

which is identical to the classical definition.

2) Performance in Extremes: There are two interesting extreme cases we can investigate:

- *Maximal Coherence*: when all n signals have pairwise mean square coherence values of 1.
- *Minimal Coherence*: when all n signals have pairwise mean square coherence values of 0.

Those cases correspond to $\mathcal{C}_s$ matrices of $\mathbf{1}$ and $\mathbf{I}$, respectively, with eigenvalues $\lambda_1 = n, 1$, respectively. Substituting those values into Eqn. (21) yields $\mathcal{C}_s^2 = 1, 0$, respectively. These results are consistent with the the new interpretation of mean square coherence: a set of signals that are completely coherent can all be perfectly explained by a single input while signals that are are incoherent cannot be explained by a single input.

TABLE I: Textures used in manipulation experiments.

texture	description
A	smooth masonite
B	masonite with 1.59mm holes, 6.35mm grid
C	masonite with 3.18mm holes, 6.35mm grid
D	silicone sensor skin texture (1.6mm dia. x 2mm tall)
E	masonite with 6.35mm wide rectangular slats
F	60 grit sandpaper
G	150 grit sandpaper
H	400 grit sandpaper

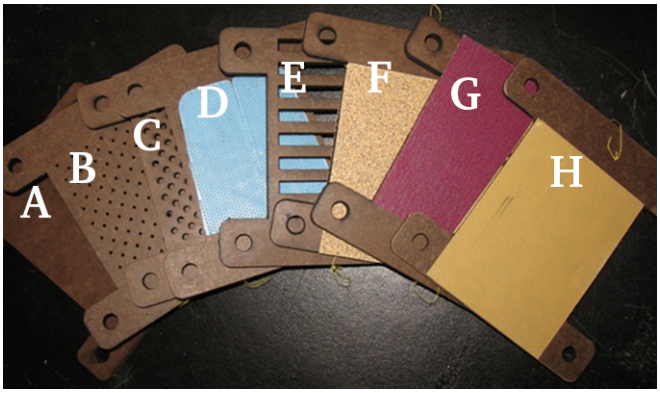

Fig. 3: Eight texture plates used in slip classification experiments. Descriptions included in Table I

III. Experimental Validation

In order to analyze and compare the performance of generalized mean square coherence as a basis for slip classification, we performed a variety of manipulations designed to evince different slip conditions. The experiments used two tactile array sensing suites with different transduction mechanisms in order to investigate the method's generalizability to other sensor arrays. In this section the sensor suites and the corresponding experiments are described.

A. BioTac™

The first sensor system used is the commerically available BioTac™ fingertip from Syntouch, LLC. A full discussion of the sensor is beyond the scope of the paper; more information can be found at [21]. For the puproses of this analysis, the sensor array consists of the high-frequency pressure signals available from two BioTacs mounted on opposing fingers of a Motion Control Inc. hand (Fig. 1). The pressure signal, P_{ac}, is sampled at 2.2kHz with an integrated 10Hz high-pass filter. These signals are synchronized between fingers by the included sampling electronics.

Four manipulations using eight different texture plates (Table I and Fig. 3) were performed using the BioTac sensors. The Motion Control hand with attached sensors was rigidly mounted on a stand (Figs. 1 and 4) and passively closed on various texture plates. The following actions were performed under two different speeds:

- passively pulled through the fingertips using added weight;
- rubbed by an external gripper manually actuated along a vertical slide as in Fig. 4a, with both soft and hard

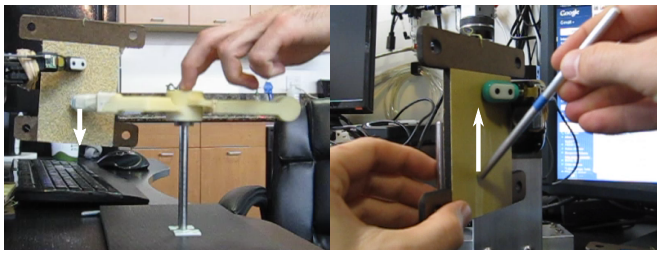

(a) (b)

Fig. 4: Two of the four BioTac experiments: (a) a passively loaded manual gripper slips against the held plate and (b) a stylus is rubbed across the held textured plate.

interfaces;

- braced against a vertical shaft while vibrations were produced by manually rubbing with an aluminum stylus (Fig. 4b).

B. PVDF experiments

The second sensor system is a custom designed polyvinylidene flouride (PVDF) piezoelectric system integrated into a soft fingertip (Fig. 5). Each fingertip has an embedded digital acquisition chip (Analog Devices AD7608) which is capable of simultaneously sampling up to eight analog channels at up to 250kHz. Due to bandwidth limitations of the entire sampling system, each AD7608 is set sample at 6.25kHz using a built-in anti-aliasing filter at 3.125kHz. Eight separate PVDF strips are attached directly to the high impedance inputs of the AD7608 in a voltage measurement configuration, and arranged as shown in Fig. 5a. Up to three fingertips are connected via SPI to a microcontroller (Microchip dsPIC33FJ32MC304) which controls and synchronizes sampling and communicates via USB to a PC for data collection.

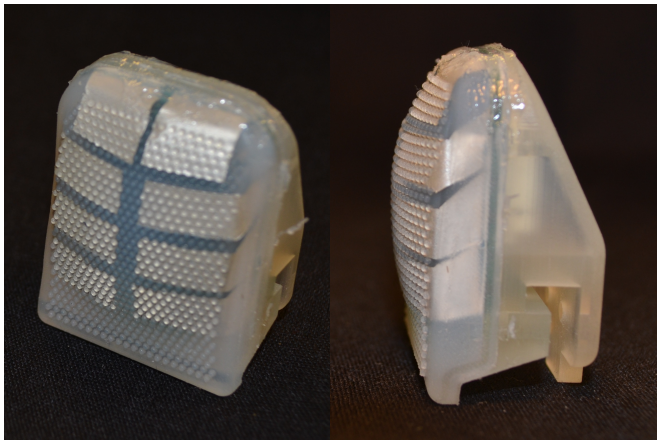

(a) (b)

Fig. 5: Tactile array sensor with eight embedded PVDF strips in a) isometric view and b) profile. The sensor package can be mounted on the benchtop slip test apparatus in Fig. 6

The PVDF-based sensor fingertips are mounted to the bench-top test apparatus shown in Fig. 6. The apparatus

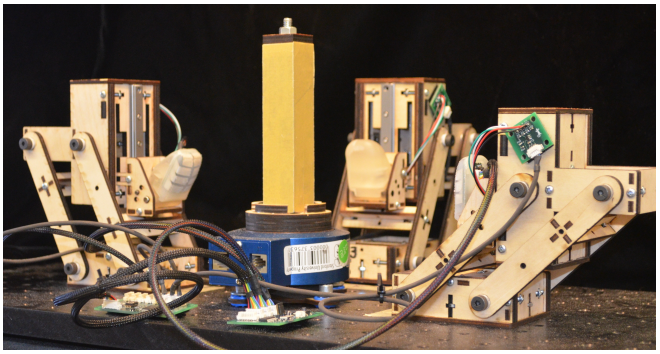

(a) Side view of the slip-classification testbed

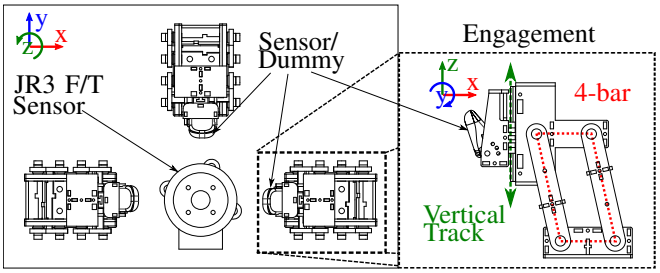

(b) Details of the slip testbed

Fig. 6: a) The benchtop slip-classification testbed used in PVDF sensor experiments. Slippage may be produced between a test object and up to three prototype tactile sensors and/or external "environment objects". b) Schematic top- and side-views show the arrangement and motion of engagement mechanisms.

includes three engagement mechanisms arranged at 0°, 90°, and 180° around a JR3 6-axis force/torque sensor (JR3 Inc, Woodland Ca) (Fig. 6b). Each engagement mechanism consists of a vertical track mounted on a parallel four-bar mechanism and is used to bring a PVDF fingertip or an unsensorized "environment" object into contact with a "held" object mounted to the force/torque sensor (Fig. 6b inset). A spring loaded mechanism allows passive variations in the generated contact force.

The data presented here are from two experiments, each performed at two contact forces. A sensorized fingertip and an unsensorized polyurethane blank (hardness shore 90D) are mounted and brought into contact with a textured "held" object. Then,

- the sensor fingertip is manually moved along the vertical track, producing object/hand slip;
- the polyurethane blank is manually moved along the vertical track, producing object/world slip.

The sandpaper textures (*F-H*) were used for the PVDF benchtop tests. They were modified by adding a light layer of spray-on rubber coating (PlastiDip Spray™) to dull the sharp edges of the sandpaper grit. This prevents excessive wear of the sensors without significantly affecting the sample's roughness.

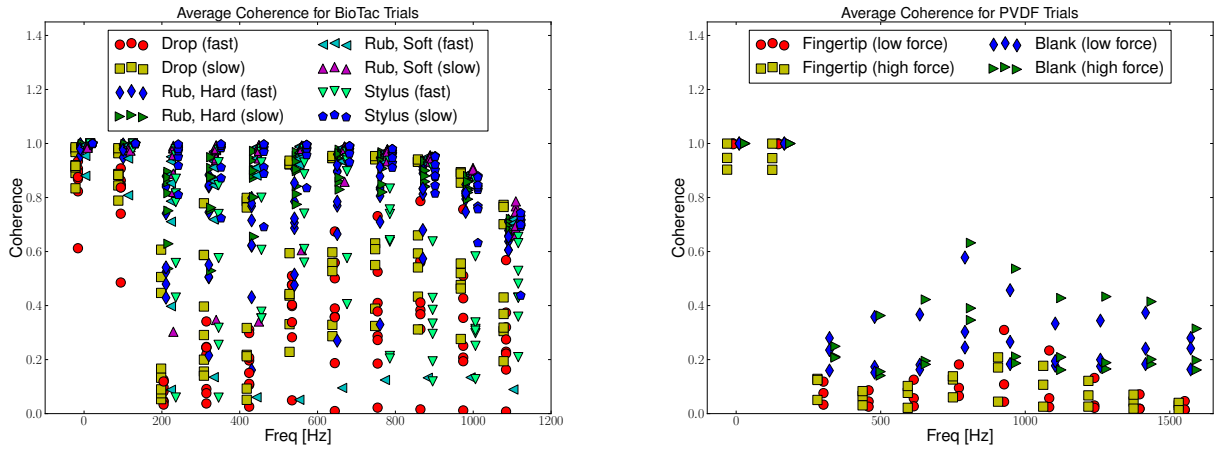

(a) (b)

Fig. 7: Coherence values for each experiment/texture combination averaged over all trials for a range of frequencies.

IV. Results

Each experiment and texture combination was performed 10 times. BioTac experiments were additionally performed at two speeds and PVDF experiments performed at two levels of passive contact loading, resulting in a total of 640 BioTac trials and 120 PVDF trials.

The complex coherence matrix for each trial was estimated using the FFT and Welch's algorithm [20], from which the mean squared coherence value was computed using Eqn. (21) at each frequency available from the FFT. The result was averaged across the 10 trials to get an expected coherence for a particular experiment/texture/speed/force combination.

Fig. 7 shows all the trial average results for the two sensors and the associated experiments. Each point is the average across all trials for a particular experiment with color/shape indicating the experiment. Although the distributions of results from the two sensors are noticeably different, in both cases instances of object/world slip have higher coherence values than instances of object/hand slip.

This trend is made clearer in Fig. 8. The regions defined by the mean and standard deviation of the examples of each type of slip are displayed instead of trial averages. The amount of overlap is indicative of how well coherence values can be used to classify slip. In the BioTac data (Fig. 8a) there is significantly more overlap at higher frequencies in contrast to very good separation in the 200-300Hz region. There is also a frequency dependence in the PVDF data (Fig. 8b), with better separation at higher frequencies and the worst separation occurring at 900-1100Hz.

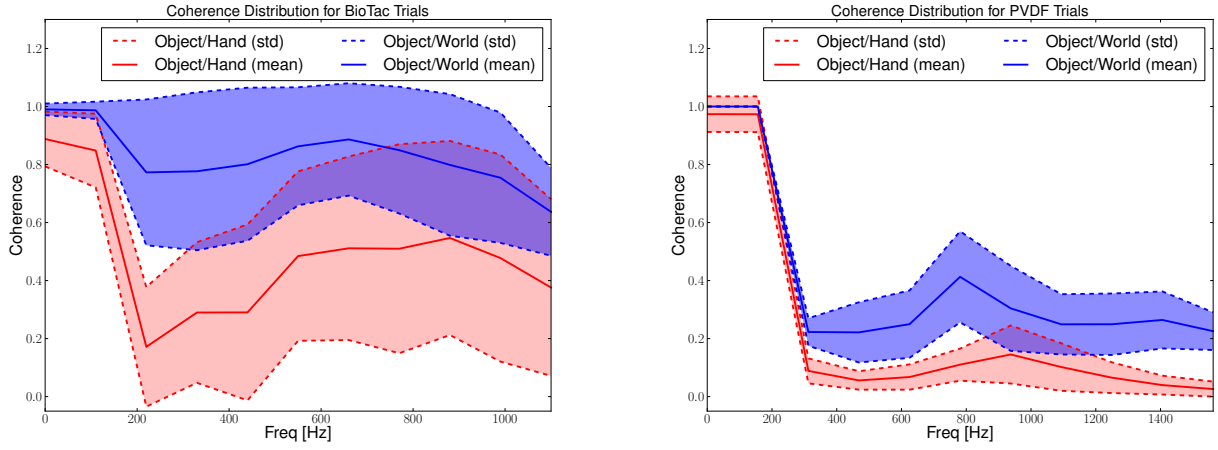

(a) (b)

Fig. 8: Regions generated by plotting the mean and standard deviation of the coherence for all trials of the given slip type (object/hand or object/world). The trend of higher coherence values during object/world slip is clear and present in the data from both sensors.

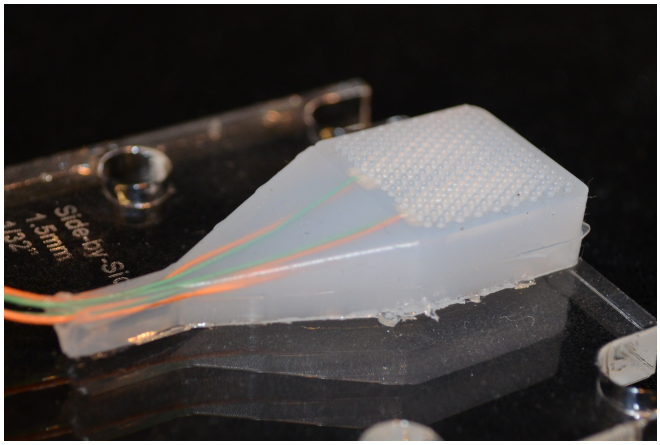

Fig. 9: A simple two-sensor test block. Two PVDF strips are embedded in silicone 4.5mm below a textured surface consisting of 1mm×0.8mm dia. posts with hemispherical ends.

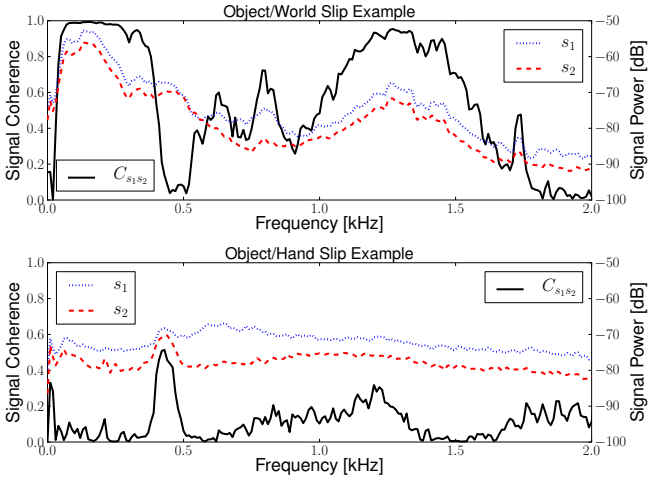

Fig. 10: Power spectral density and coherence for two-sensor test arrays. Top: data from an object/world slip condition. Bottom: data from an object/hand slip condition. Note the relatively high coherence near 450Hz and 1200Hz during both slip conditions. These frequencies correspond closely to the bulk vibration modes of a block of silicone.

V. Discussion

As expected based on the coherence analysis presented in Section II, the examples of object/world slip produce coherence that is generally higher than that produced during object/hand slip. In the data from each sensor there are frequency ranges which have good separation between object/world slip and object/hand slip coherence values and could therefore be used for classifying slip interface. However, the separation is dependent on frequency, and the well-separated frequency ranges are different for the two sensors.

A goal of this research is to develop physically motivated *signal features* for slip classification which generalize across sensors and contact conditions. For this reason frequency dependent results are undesirable unless they can be predicted based on the sensor design and are not functions of the contact conditions, which may be unknown or uncertain during manipulation tasks.

Because coherence values are large at frequencies that have consistent relative phasing between signals, sensors embedded in soft polymers may experience artificially high coherence values at frequencies corresponding to bulk vibration modes of the sensor. This phenomenon was observed in early tests using PVDF strips embedded in blocks of silicone (Fig. 9). An FEA analysis performed in Solidworks indicated that first the 5 bulk vibration modes of cuboid test blocks of the same dimensions were clustered around 500Hz and 1250Hz. Simple tests in which a texture plate was manually dragged across a test block (object/hand slip) or held against the test block and rubbed with a stylus (object/world slip) were performed. High coherence values were observed in both cases near the bulk vibration frequencies (Fig. 10) indicating that those frequency ranges do not provide information pertaining to slip interface classification.

When this method is applied to other sensors suites, a knowledge of modes common to all sensors in the array, whether from bulk vibration modes of the finger material or other sources, can be used to exclude certain frequency ranges from coherence calculations. This result also suggests that certain frequency ranges corresponding to interactions with a textured sensor surface may be especially useful for coherence analysis. However, this has not yet been experimentally confirmed and is a further avenue of work.

The method presented here supports a very liberal definition of "sensor array." Typically a tactile sensor array is a physically contiguous set of sensors embedded in or mounted to a single block of material. These coherence methods can use *distributed* arrays of tactile sensors, such as the P_{ac} signals from two separate BioTac sensors. The only requirement is that distributed sensors all be in physical contact with the held object. While there is no specific evidence of this *inter-finger* sensor fusion in human biology, robotic systems using this method are able to take advantage of vibrations picked up on all surfaces containing tactile sensors that are in contact with a held object.

VI. Conclusions and Future Work

We have presented an analytical generalization of *mean square coherence*, previously only defined for two signals, which extends to populations of n sensors. This generalization is a result of examining the degree to which individual sensors are sampling a common underlying signal. It is consistent with the classical definition when $n = 2$ and can be calculated via eigenvalue analysis of the complex coherence matrix of the population.

Using a linear system model of the interaction between the environment, a held object, and an array of tactile sensors in a robot hand we have demonstrated how mean square coherence values can be used to determine slip interface. The efficacy of this method was investigated using two different sensor suites and a variety of textures and slip conditions. Results from these experiments indicate that coherence based

measures can be used to classify slip type and should generalize well to other sensors and situations.

The bench-top testbed used with the PVDF sensors has many additional capabilities, including a variety of witness sensors and the ability to generate slip independently on two fingers and a third object/world interface. Future work will explore the ability of coherence based methods to determine which interfaces are experiencing slip in more complex situations, e.g. slip at one object/finger interface at the same time as slip at the object/world interface. Additionally, extending these methods to a real-time system will require investigating how much data is needed to reliably classify slip, and what delays are introduced between the onset of slip and a reliable classification.

REFERENCES

[1] M. R. Cutkosky, R. D. Howe, and W. R. Provancher, "Force and Tactile Sensors," in *Springer Handbook of Robotics* (B. Siciliano and O. Khatib, eds.), ch. 22, pp. 455–476, Berlin, Heidelberg: Springer Verlag, 2008.

[2] R. S. Dahiya, G. Metta, M. Valle, and G. Sandini, "Tactile Sensing From Humans to Humanoids," *IEEE Transactions on Robotics*, vol. 26, no. 1, pp. 1–20, 2010.

[3] H. Yousef, M. Boukallel, and K. Althoefer, "Tactile sensing for dexterous in-hand manipulation in roboticsA review," *Sensors and Actuators A: Physical*, vol. 167, pp. 171–187, June 2011.

[4] R. D. Howe and M. R. Cutkosky, "Sensing skin acceleration for slip and texture perception," in *IEEE International Conference on Robotics and Automation*, pp. 145–150, IEEE Comput. Soc. Press, 1989.

[5] C. Melchiorri, "Slip Detection and Control Using Tactile and Force Sensors," *IEEE/ASME Transactions on Mechatronics*, vol. 5, no. 3, pp. 235–243, 2000.

[6] J. Edwards, J. Lawry, J. Rossiter, and C. Melhuish, "Extracting textural features from tactile sensors.," *Bioinspiration & Biomimetics*, vol. 3, Sept. 2008.

[7] J. M. Romano, K. Hsiao, G. Niemayer, S. Chitta, and K. J. Kuchenbecker, "Human-Inspired Robotic Grasp Control with Tactile Sensing," *IEEE Transactions on Robotics*, no. 99, pp. 1–13, 2011.

[8] R. D. Howe and M. R. Cutkosky, "Dynamic tactile sensing: perception of fine surface features with stress rate sensing," *IEEE Transactions on Robotics and Automation*, vol. 9, pp. 140–151, Apr. 1993.

[9] P. A. Schmidt, E. Maël, and R. P. Würtz, "A sensor for dynamic tactile information with applications in humanrobot interaction and object exploration," *Robotics and Autonomous Systems*, vol. 54, pp. 1005–1014, Dec. 2006.

[10] H. Muhammad, C. Recchiuto, C. M. Oddo, L. Beccai, C. Anthony, M. Adams, M. C. Carrozza, and M. Ward, "A capacitive tactile sensor array for surface texture discrimination," *Microelectronic Engineering*, vol. 88, pp. 1811–1813, Aug. 2011.

[11] C. M. Oddo, M. Controzzi, L. Beccai, C. Cipriani, and M. C. Carrozza, "Roughness Encoding for Discrimination of Surfaces in Artificial Active-Touch," *IEEE Transactions on Robotics*, vol. 27, no. 3, pp. 522–533, 2011.

[12] J. A. Fishel and G. E. Loeb, "Bayesian Exploration for Intelligent Identification of Textures," *Frontiers in Neurorobotics*, vol. 6, pp. 1–20, Jan. 2012.

[13] R. S. Johansson and J. R. Flanagan, "Coding and use of tactile signals from the fingertips in object manipulation tasks.," *Nature Reviews: Neuroscience*, vol. 10, pp. 345–359, May 2009.

[14] A. J. Brisben, S. S. Hsiao, and K. O. Johnson, "Detection of Vibration Transmitted Through an Object Grasped in the Hand," *Journal of Neurophysiology*, vol. 81, pp. 1548–1558, 1999.

[15] B. Heyneman and M. R. Cutkosky, "Biologically inspired tactile classification of object-hand and object-world interactions," in *IEEE International Conference on Robotics and Biomimetics*, 2012.

[16] R. S. Johansson and I. Birznieks, "First spikes in ensembles of human tactile afferents code complex spatial fingertip events," *Nature Neuroscience*, vol. 7, no. 2, pp. 170–177, 2004.

[17] J. Fox and T. Daniel, "A neural basis for gyroscopic force measurement in the halteres of Holorusia.," *Journal of Comparative Physiology A*, vol. 194, pp. 887–97, Oct. 2008.

[18] J. Greenstein, P. Kavanagh, and M. J. Rowe, "Phase coherence in vibration-induced responses of tactile fibres associated with pacinian corpuscle receptors in the cat," *The Journal of Physiology*, vol. 386, pp. 263–275, 1987.

[19] C. H. Lin, T. W. Erickson, J. A. Fishel, N. Wettels, and G. E. Loeb, "Signal Processing and Fabrication of a Biomimetic Tactile Sensor Array with Thermal, Force and Microvibration Modalities," in *IEEE International Conference on Robotics and Biomimetics*, 2009.

[20] S. L. J. Marple, *Digital Spectral Analysis: with applications*. Englewood Cliffs, NJ: Prentice-Hall, 1987.

[21] "Technology Overview," 2013.